Magnetic propulsion of microspheres at liquid-glass interfaces

Geir Helgesen

Citation: Journal of Applied Physics **123**, 064902 (2018); doi: 10.1063/1.5011350
View online: https://doi.org/10.1063/1.5011350
View Table of Contents: http://aip.scitation.org/toc/jap/123/6
Published by the American Institute of Physics

Magnetic propulsion of microspheres at liquid-glass interfaces

Geir Helgesen[a)]
Physics Department, Institute for Energy Technology, NO-2027 Kjeller, Norway

(Received 31 October 2017; accepted 25 January 2018; published online 13 February 2018)

Bio-coated, magnetic microspheres have many applications in biotechnology and medical technology as a tool to separate and extract cells or molecules in a water solution by applying external strong magnetic field gradients. However, magnetic microspheres with or without attached cargo can also be separated in the liquid solution if they are exposed to alternating or rotating, relatively weak magnetic fields. Microspheres that have a higher density than the liquid will approach the bottom surface of the sample cell, and then a combination of viscous and surface frictional forces can propel the magnetic microspheres along the surface in a direction perpendicular to the axis of field rotation. Experiments demonstrating this type of magnetic propulsion are shown, and the forces active in the process are discussed. The motion of particles inside sample cells that were tilted relative to the horizontal direction was studied, and the variation of propulsion velocity as a function of tilt angle was used to find the values of different viscous and mechanical parameters of motion. Propulsion speeds of up to 5 μm/s were observed and were found to be caused by a partly rolling and partly slipping motion of rotating microspheres with a slipping coefficient near 0.6. https://doi.org/10.1063/1.5011350

I. INTRODUCTION

In magnetophoresis, paramagnetic or ferromagnetic micro- and nanoparticles that are dispersed in a fluid are forced to move due to external magnetic field gradients.[1] Such magnetic microbeads are often made by emulsion polymerization, and also, a wide range of other preparation techniques exist.[2] The magnetic propulsion force acting on microbeads will depend on their magnetic moment m, which is normally proportional to their volume, the strength of the externally applied field H, and the field gradient ∇H, and it will pull them into regions of stronger field. For small particles, this process is very slow due to the competition between magnetic propulsion, viscous forces, and Brownian motion. However, by applying relatively weak, rotating magnetic fields and utilizing microsphere-surface interaction forces, the magnetic propulsion speeds can be controlled and possibly increased relative to applying static magnetic fields. This method will be discussed below after a summary of the current status of magnetic propulsion.

In some applications, micro-swimmers can propel due to their ability to convert chemical energy or heat in their surroundings into a directed motion.[3] However, for micrometer sized particles, the speeds will be low due to viscous effects since the Reynolds number Re is very small ($Re \ll 1$). For applications in microfluidics and biotechnology, the liquid volumes are usually also small, which means that the magnetic particles are close to walls. The effect of a wall is normally to slow down any motion due to an increased effective fluid viscosity near the wall. In some cases, the presence of a wall can also be utilized in order to enhance the propulsion. The theory of motion of particles near solid walls has been discussed in several papers.[4–6] By applying rotating magnetic fields, magnetic microbeads can be forced to rotate.[7–10] The motion of active and passive rotors has been discussed by Fily *et al.*,[11] and magnetic colloidal surface walkers[12] and tumblers[13] have been reported. Biocompatible ferrofluids inside microfluidic platforms have been used to manipulate and separate out nonmagnetic microparticles and live cells.[14] The current status of how to activate soft matter with magnetic torque has been reviewed by Erb *et al.*[15]

The motion of small suspended particles near walls can involve competition among viscous forces, frictional forces, electrostatic forces, and gravitational forces. The rolling motion of non-colloidal spheres down inclined planes inside fluids has been discussed in a couple of papers. Smart *et al.*[16] made a theoretical model and did experiments for rough spheres rolling on planes at various inclinations and showed the effect of surface roughness. Galvin *et al.*[17] did a similar study using spheres that had two separate scales with distinct distributions of the surface roughness elements. They managed to find a transition from smaller to larger separation heights above the inclined plane, and this was dependent on the inclination angle and the roughness scales. The inertial lift force on a rigid sphere in a linear shear flow field near a wall was calculated by Cherukat and McLaughlin.[18] Later, Krishnan and Leighton[19] and King and Leighton[20] extended these calculations and measured the transition from rolling to translation with slip along the surface. The effects of interaction between a microparticle in shear flow and charged surface patches have also been studied.[21] Agayan *et al.*[22] used optical tweezers to trap magnetic microspheres near a surface and exposed the particles to rotating magnetic fields.

[a)]geir.helgesen@ife.no

The particles then got a new equilibrium position, which was displaced relative to the center of the optical trap, and the authors studied how the rolling and slipping of the microspheres depended on the magnetic rotation rate and surface properties. They also measured the same for free, non-trapped microspheres on a glass surface and observed a shift in the direction of motion of the particles relative to the plane of the rotating field in both cases. This was interpreted as a shift of the direction of the spheres' magnetic moment away from the plane of rotation. Recently, it was proposed that the motion of magnetic beads on inclined planes can be used as a technique for size separation of the beads.[23] Martinez-Pedrero and Tierno[8] showed that carpets of magnetically driven rotating beads can be used to carry cargo such as cells and modeled the translational motion as purely due to hydrodynamic effects.[9] In the present study, it will be shown that surface contact forces also play an important role in near-surface propulsion.

II. EXPERIMENTAL DETAILS

The experimental setup consisted of an optical microscope (Nikon Optiphot), a custom made set of three orthogonal pairs of current carrying coils, and a custom made computer controlled power supply for the magnet coils. A digital-to-analogue converter (Measurement Computing Systems), which was controlled by a PC, supplied the input signals for the power supply. The oscillating digital signals were generated in Labview. The microparticle motion was recorded on a PC using a C-mounted DinoEye USB video camera and the DinoCapture software. The amplitudes and phases of the coil currents were monitored using a digital oscilloscope (GW-INSTEK) and three separate multimeters. Images from the videos were extracted at specific times using the Cyberlink PowerDirector program. Particle tracks were also extracted directly from AVI-video files using the Video-spot-tracker-v08 software (CISMM at UNC Chapel Hill, www.cs.unc.edu/~nanowork/cismm/). Figures 1(a)–1(c) show the coil system, the glass sample cell, and the microspheres inside.

The magnetic microparticles were dispersed in de-ionized water containing 0.1% SDS (Sodium Dodecyl Sulfate) surfactant and placed in between a microscope glass slide and a cover slide. The separation between the slides was controlled by using one or two layers of double-sided tape as spacers along two of the sides of the cell (giving a plate separation of $h \approx 85\,\mu$m or $170\,\mu$m). All the sides of this thin cell were sealed using epoxy glue. Typical coil current amplitude used was $I = 1.4$ A that gave a magnetic field amplitude of about $H = 1100$ A/m.

The microspheres used in the current experiments were provided by the Ugelstad laboratory at NTNU/SINTEF (Trondheim, Norway). They were made of polystyrene, had an iron content of about 24% (magnetite Fe_3O_4/maghemite Fe_2O_3), and had a density of $\rho_s \approx 1.6\,\mathrm{g/cm^3}$. Spheres of diameters $d = 30\,\mu$m, $4.7\,\mu$m, $3.5\,\mu$m, and $1.5\,\mu$m were used. Similar particles have been characterized in more detail by Fonnum *et al.*,[24] who found paramagnetic mass susceptibilities in the range of $\chi_m = 55\text{–}100 \times 10^{-5}$ $\mathrm{m^3/kg}$, and these authors also found that the microspheres contained magnetic nanoparticles of size about 8 nm with inter-particle magnetic interactions, thus giving rise to nanoparticle clusters.

Sample cells containing a very dilute mixture of microspheres were mounted in the coil system, and the motions of particles with and without a rotating magnetic field were recorded for several inclinations of the whole microscope system. A simple tilt table was used for this purpose. The recorded videos were used to extract propulsion velocities. All velocity measurements were repeated several times using different microspheres within a sample and also using different sample cells. The average velocity was found to vary slightly among equally sized particles. Thus, the reported data correspond to average velocity values with standard deviations for individual microspheres.

III. THEORETICAL CONSIDERATIONS

Janssen *et al.*[7] have shown that the average angular rotation frequency of a microbead, ω_b, depended linearly on the magnetic field rotation frequency $f_\mathrm{H} = \omega_\mathrm{H}/2\pi$ up to a critical frequency f_H^{crit}. Above that, ω_b decreased gradually with increasing f_H. This result is similar to the frequency dependence previously found for pairs of so-called magnetic holes.[25,26] Janssen *et al.* also showed that the permanent magnetic moment m_p seems to be locked to one direction of a fixed axis within the sphere. For higher frequencies, they observed that the main reason for sphere rotation was the induced magnetic moment caused by the imaginary part of the complex susceptibility $\chi''(\omega_H)$. The angular direction φ_b of a fixed axis within the bead could be modeled as

$$m_\mathrm{p}\mu_0 H \sin(\omega_\mathrm{H} t - \varphi_\mathrm{b}) + \chi''(\omega_H)\mu_0 H^2 V = \lambda \frac{\mathrm{d}\varphi_\mathrm{b}}{\mathrm{d}t}, \quad (1)$$

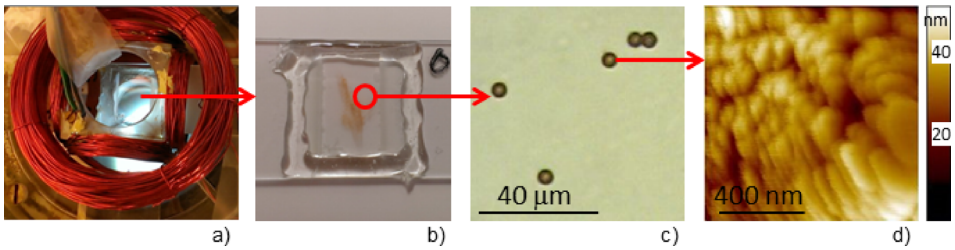

FIG. 1. (a) The coil system used in the present study for creating three separate magnetic fields that can rotate in the *XY*-, *XZ*-, or *YZ*-planes. Part of the sample cell can be seen inside the coils. (b) The sealed sample with microspheres on a 25 mm wide glass slide. (c) Microscopy image of the 4.7 μm magnetic microspheres. (d) AFM surface scan of a dry microsphere. Similar scans were used to find the surface roughness (see Part IV). This scan has been corrected for the spherical shape of the particle.

with V being the volume of the bead and λ a hydrodynamic drag factor. For magnetic monodisperse nanoparticles, the imaginary part of the susceptibility is

$$\chi''(\omega_H) = \chi_0 \frac{\omega_H \tau_m}{1 + \omega_H^2 \tau_m^2}, \tag{2}$$

with χ_0 being the static field susceptibility and τ_m the magnetic relaxation time, which is mainly controlled by the nano-domain anisotropy energy. Inside the beads, there was a broad distribution of nanoparticles, which was assumed to be log-normal by the authors of Ref. 7, and this was interpreted as the reason for a broad peak in bead average rotation frequency $\Omega = \langle \frac{d\varphi_b}{dt} \rangle$ at higher field rotation frequencies.

For microparticles in the present size range, the most relevant parameter for characterizing their motion is the Reynolds number of sedimentation, i.e., for a sphere of radius a falling freely in a liquid far away from disturbing walls, $Re_s = \frac{U_s a}{\nu}$. Here, $U_s = \frac{2}{9}\Delta\rho g a^2/\eta_0$ is the sedimentation velocity of the sphere with $\Delta\rho = \rho_s - \rho_l = 600\,\mathrm{kg/m^3}$ being the density difference between microspheres and water in the present case, $g = 9.81\,\mathrm{m/s^2}$ the acceleration of gravity, and $\eta_0 = 0.80$ mPa s and $\nu = 8.0 \times 10^{-7}\,\mathrm{m^2/s}$ the dynamic viscosity and kinematic viscosity, respectively, of water at temperature $T = 30\,^\circ\mathrm{C}$. From this, $U_s = 9.0\,\mu\mathrm{m/s}$ and $Re_s = 3 \times 10^{-5}$. Thus, all motions are strongly damped.

When a non-rotating sphere is translated at a velocity $\mathbf{U}_x$ in the x-direction parallel to a wall, there will be a viscous drag force acting in the direction opposite to the motion[27]

$$\mathbf{F}_x^t = -6\pi a \eta_0 \cdot f_{xx}^t \cdot \mathbf{U}_x, \tag{3}$$

with a translational drag correction coefficient $f_{xx}^t = f_{xx}^t\left(\frac{s}{a}\right)$ that is dependent on the distance s from the sphere center to the wall. Similarly, for a sphere that is kept fixed, but is rotating at angular velocity $\mathbf{\Omega}_y$ about the y–axis direction, there will be a viscous force[27]

$$\mathbf{F}_x^r = 6\pi a^2 \eta_0 \cdot f_{xy}^r \cdot \mathbf{\Omega}_y \tag{4}$$

that is trying to translate the sphere along the x-direction. Here, $f_{xy}^r = f_{xy}^r\left(\frac{s}{a}\right)$ is the corresponding rotational-translational drag correction coefficient.

For a sphere rotating very close to the wall with a separation of $\delta = s - a$ between the surface of the sphere and the flat surface of the wall, the correction factor due to translation, f_{xx}^t, and the correction factor due to rotation, f_{xy}^r, can be approximated by[28,29]

$$f_{xx}^t \approx \frac{8}{15}\ln\left(\frac{a}{\delta}\right) + 0.9588 = -\frac{8}{15}\ln\left(\frac{s}{a} - 1\right) + 0.9588, \tag{5}$$

$$f_{xy}^r \approx \frac{2}{15}\ln\left(\frac{a}{\delta}\right) - 0.2526 = -\frac{2}{15}\ln\left(\frac{s}{a} - 1\right) - 0.2526. \tag{6}$$

As an example, the factors f_{xx}^t and f_{xy}^r increase from 2.56 and 0.147, respectively, at $\frac{\delta}{a} = 0.05$ to 5.87 and 0.975 at $\frac{\delta}{a} = 10^{-4}$.

Now consider the situation with a magnetic microsphere located near a planar surface, which is tilted an angle α relative to the horizontal direction and with the x–axis of the coordinate system pointing along the surface in the tilt direction, denoted "uphill" from here. This is shown in Fig. 2. The y–axis is along the surface in the perpendicular in-plane direction. The sphere is acted on by an external, rotating magnetic field that is forcing it to move up or down the inclined plane. The forces acting on the sphere (see Fig. 2) are gravity $W_g = \frac{4}{3}\pi a^3 \Delta\rho g$, a surface normal force N_c in the contact point between the sphere and the surface, a lift force L_h due to a hydrodynamic lift at the finite Reynolds number, a friction force $F_f = \mu_k N_c$ acting in the contact point parallel to the surface with μ_k being the kinetic friction coefficient, and a viscous drag force F_h due to the translation and rotation of the sphere. This drag is opposite to the direction of motion. The equations for balance of forces parallel and perpendicular to the surface are $\varepsilon F_f + F_h - W_g \sin\alpha = 0$ and $N_c + L_h - W_g \cos\alpha = 0$ with $\varepsilon = +1$ for a sphere moving uphill and $\varepsilon = -1$ for a sphere moving in the opposite direction, i.e., downhill. Combining these equations, one finds

$$\varepsilon\mu_k(W_g \cos\alpha - L_h) + F_h - W_g \sin\alpha = 0. \tag{7}$$

The drag force is due to translation and rotation of the sphere $F_h = F_h^t + F_h^r$ with the latter two given by Eqs. (3) and (4).

Now assume that the sphere is rotating with a positive angular frequency Ω_y, having an uphill velocity U_x. The motion is partly rolling and partly slipping, and this "skipping" can be modeled through a slipping coefficient γ as $U_x = \gamma a \Omega_y$.[23] Then

$$\begin{aligned} F_h &= 6\pi\eta_0 a\left(-f_{xx}^t \cdot U_x + f_{xy}^r \cdot a\Omega_y\right) \\ &= -6\pi\eta_0 a U_x\left(f_{xx}^t - \frac{1}{\gamma}\cdot f_{xy}^r\right). \end{aligned} \tag{8}$$

When a rigid sphere is moving near a flat surface, there will be a small lift force on the sphere pushing it away from the surface in the surface-normal z–direction. This will happen when the surface is within the disturbance flow-field of the sphere.[18] In general, if a particle is rotating and translating near a wall, the hydrodynamic lift force L_h will be

$$L_h(\Omega, \gamma) = \rho a^4 \Omega^2\left(\lambda_2 - \lambda_3\gamma + \lambda_1\gamma^2\right), \tag{9}$$

where $\lambda_1 = 1.755$, $\lambda_2 = 0.546$, and $\lambda_3 = -2.038$ are the lift coefficients.[19,23] Combining Eqs. (7) and (8), one finds the force balance[23]

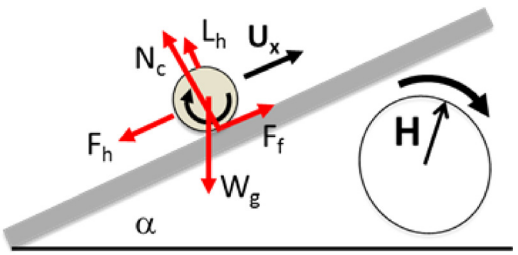

FIG. 2. Schematic diagram of a microsphere moving at velocity U_x near an interface that is tilted at an angle α. The forces acting are gravitational force W_g, surface normal contact force N_c, surface friction force F_f, hydrodynamic lift force L_h, and viscous drag force F_h.

$$\varepsilon\mu_k(W_g\cos\alpha - L_h) - 6\pi\eta_0 a U_x\left(f_{xx}^t - \frac{1}{\gamma}\cdot f_{xy}^r\right) - W_g\sin\alpha = 0. \tag{10}$$

Inserting values for tilt angle α ($5° \le \alpha \le 30°$), slipping coefficient $0 \le \gamma \le 1$, and angular velocity of rotation $\Omega \sim 1\,\mathrm{s}^{-1}$, one finds that the lift force L_h is typically a factor of 10^{-7} smaller than the gravitational force $W_g \approx 0.3$ pN and thus can be neglected. Then, the velocity of the microspheres is given by

$$U_x = U_s \cdot \frac{\varepsilon\mu_k\cos\alpha - \sin\alpha}{f_{xx}^t - \frac{1}{\gamma}\cdot f_{xy}^r}, \tag{11}$$

where U_s is the sedimentation velocity defined above and with $\varepsilon = +1$ for uphill motion and $\varepsilon = -1$ for downhill motion. For small tilt angles α, one finds a linear U_x vs. α relationship $U_x \approx \frac{U_s}{f_{xx}^t - \frac{1}{\gamma}f_{xy}^r}(\varepsilon\mu_k - \alpha)$.

As will be shown below, the uphill motion vanishes, $U_x = 0$, at a certain critical angle α_{crit}, and then $\gamma = 0$. Then, the force balance Eq. (10) is replaced by $W_g(\mu_k\cos\alpha - \sin\alpha) - 6\pi\eta_0 a^2 f_{xy}^r \cdot \Omega_y = 0$, and the kinetic friction coefficient can be found as

$$\mu_k = \tan\alpha_{crit} + \frac{a}{U_s\cdot\cos\alpha_{crit}}\cdot f_{xy}^r\cdot\Omega_y. \tag{12}$$

IV. RESULTS AND DISCUSSION

Figure 3 shows recorded traces for the motion of two microspheres moving concomitantly inside a horizontal glass sample cell of thickness about 85 μm (data extracted from Video 1 in the supplementary material). The direction of motion is dominantly parallel to the plane formed by the rotating magnetic field, but there is also a small fluctuating component perpendicular to this plane. This may partly be due to Brownian motions and partly due to tiny obstacles on the glass surface. For much smaller particles ($d \le 1.5\,\mu$m), the Brownian component was dominating and the propulsion was very weak for the magnetic field strengths used in the current study ($H < 2$ kA/m). Some variations in the velocities among equally sized particles were observed, which may be attributed to variations of the amount of paramagnetic material (magnetite/maghemite) inside each sphere. Also, permanent sticking of a few spheres to the glass surface was observed. The ability of bringing particles almost back to their starting position after being moved around for 200 s (8×25 s), as shown in Fig. 3, indicates the level of precision for control of the particles using the current method.

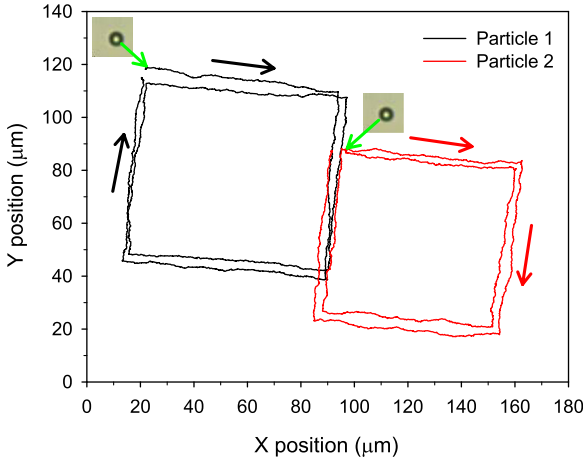

FIG. 3. The traces of two $d = 3.5\,\mu$m spheres being propelled by a rotating magnetic field at the interface between water and a horizontal glass surface. The field amplitude was $H = 1.1$ kA/m rotating in the *XZ*- or *YZ*- planes, and the rotation frequency $f_H = 100$ Hz. The propulsion started by applying a rotating field in the *XZ*-plane of the coil system. After 25 s, the plane of rotation was changed to the *YZ*-plane for the next 25 s. This procedure was repeated using the opposite rotation direction within the *XZ*- and *YZ*-planes, thus bringing the particles in a continuous motion back to their starting positions. This square loop motion was then repeated a second time. Note a small misalignment between the *X*- and *Y* -axes of the coil system and those of the microscope camera. The inset images show the two particles (enlarged by 50%) near their starting positions. The particle velocity was found to be $2.6 \pm 0.2\,\mu$m/s.

It may be noted that after exposure to the magnetic field, some clustering of microspheres could be seen, and this leads to collective propulsion of rafts of particles as has recently been reported[8] or to conveyor belt modes.[9] In order to avoid collective modes or hydrodynamic coupling of several spheres, only microspheres that were well separated from each other were studied.

First, the magnetic field strength and field rotation frequency dependencies of microsphere propulsion velocity were explored. Figure 4 shows the results for $d = 4.7\,\mu$m spheres inside horizontal sample cells. The propulsion velocity increases up to about $f_H = 10$ Hz and was nearly constant above that. Even at the lowest frequency of 1 Hz, the microsphere rotation was not following the field rotation, and the sphere was not rolling on the surface without slipping, since this would correspond to a propulsion velocity of $U = \pi d \cdot f_H = 14.8\,\mu$m/s. Thus, either the rotation of the microsphere did not follow in phase with the field rotation or the sphere was strongly slipping. Most likely, it was a combination of both, as will be demonstrated in the following. As seen in Fig. 4(a), there are some variations in the average velocity among particles of the same size, which as noted above may be due to variation in their content of the magnetic material.

As the frequency increased, the rotation of the spheres was clearly not able to follow the field, and the microspheres were acted on by a time-averaged torque from the magnetic field, which seems to be nearly frequency independent for $f_H > 20$ Hz. A field rotation frequency of $f_H = 100$ Hz was used in the rest of this study. The observed frequency dependence is consistent with what have been reported by Agayan *et al.*,[22] who found an increase in velocity for magnetic spheres of diameter 9 μm for field frequency up to $f_H = 2$–3 Hz and beyond that a small decrease in velocity. Figure 4(b) shows how the velocity depends on the field strength H. According to Eq. (1), $U_x \propto H^2$ behavior might be expected for superparamagnetic microbeads with $m_p = 0$. Regression fit to the measured U_x vs. H data showed a slightly weaker dependence, $U_x \propto H^{1.9}$. For stronger fields, $H \ge 2$ kA/m, Ohmic heating in the coil system prevented measurements. Janssen *et al.*[7] measured that $\Omega \propto H^2$ for the

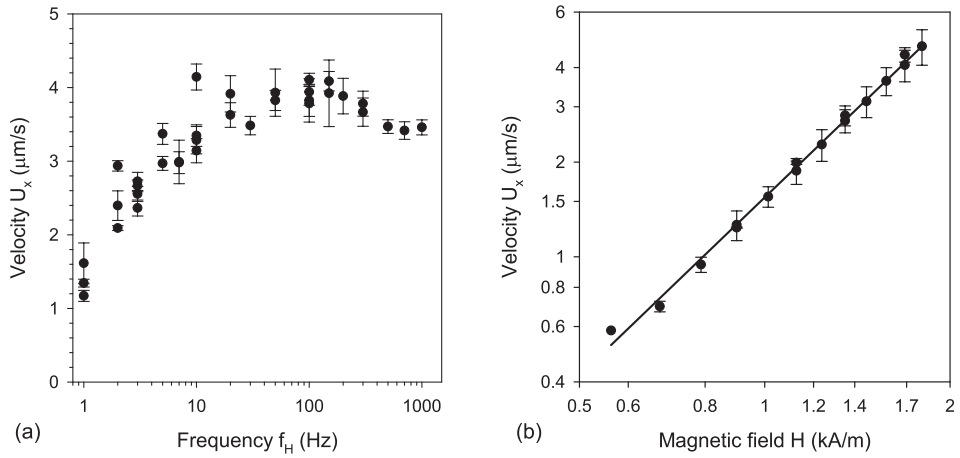

FIG. 4. (a) Propulsion velocity U_x vs. magnetic field rotation frequency f_H (logarithmic scale) for microspheres of diameter $d = 4.7\ \mu$m using a magnetic field strength of $H = 1.1$ kA/m. Each data point and its error bar represent the average value and standard deviation based on several separate measurements for one single sphere. For each frequency, typically, the velocity of two to four microspheres was measured, and the scattering of velocity data at a frequency represents the variation among similar spheres. (b) Velocity U_x as a function of field strength H at $f_H = 100$ Hz for the same spheres shown in a double-logarithmic plot. The solid regression line shows a $U_x \propto H^{1.9}$ behavior.

bead angular rotation at high frequency in their study of trapped magnetic beads.

The magnetic and viscous forces acting on particles in such micron-scale systems are difficult to measure directly. However, this can be done indirectly by comparing them to a known reference force, which can easily be found or calculated, such as the gravitational force on the particles. The importance of the effect of magnetic phase slip within the spheres[7] and the effect of slipping motion on the surface can be clarified when these forces are found. Calibrating the forces against gravity was done by placing the microscope with the coil system and sample cell on an inclined tilt table. By tilting one direction of the sample cell (here denoted the X–direction) relative to the horizontal, the microspheres will experience a component of the effective gravitational force along the surface parallel to the direction of forced motion. The propulsion velocities can then be compared to the effective sedimentation velocity due to the gravitational field alone at the same tilt angle.

Figure 5 shows the X–position of microspheres as a function of time for samples at various tilt angles in the range of $\alpha = 0°$–$22.5°$, as was shown in the schematic setup in Fig. 2. The position was measured along the tilt direction and relative to the lower edge of the microscope field-of-view. Here, the direction of H–field rotation was such that the spheres were first propelled downhill, and after a time $t = 10$ s–30 s, the direction of rotation was changed to propelling uphill. This procedure was repeated until the particles left the lower edge of the field-of-view in the microscope. In some cases, the magnetic field was turned off and the spheres were allowed to move downhill by gravity force only. This is marked by the labels "H = 0" in the figure. An example of a video recorded during one such experiment can be seen in Video 2 in the supplementary material. As can be seen, for small tilt angles, the spheres move downhill with a slightly higher speed than they move uphill, and this reduction of uphill velocity continues with increasing α until about $\alpha = 22.5°$ when the uphill motion vanishes completely. Then, the sphere was rotating in the same direction as the field (uphill, $\Omega_y > 0$) but the slipping was complete with slipping coefficient $\gamma \approx 0$. The sphere was spinning "freely" or slightly sliding down due to gravity. At the critical angle α_{crit}, the translational viscous drag force vanishes ($U_x = 0$), and only the uphill directed rotational-translational force Eq. (4) remains, which together with the force of slipping friction balances the in-plane component of gravity.

The results of these sample cell tilt experiments are presented in Fig. 6, which shows the propulsion velocity U_x as a function of the cell tilt angle α. Velocities were calculated for uphill propulsion (black circles), downhill propulsion

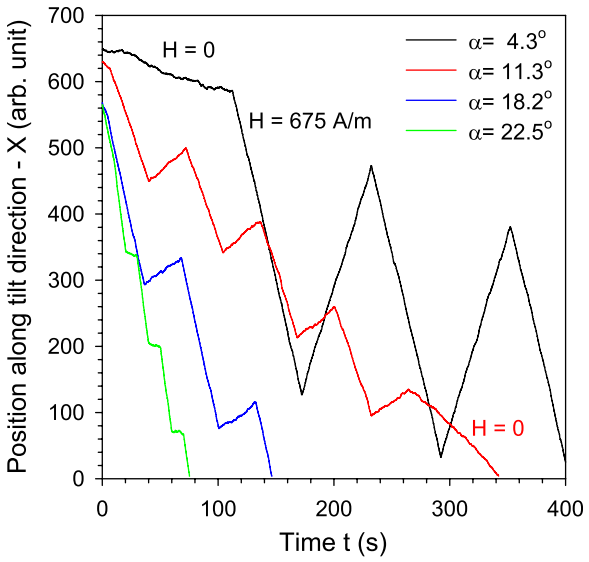

FIG. 5. Examples of the recorded traces (X-position vs. time) for $d = 4.7\ \mu$m spheres moving in a sample cell that was inclined at various angles α relative to the horizontal direction. The spheres were propelled by a rotating magnetic field of frequency $f = 100$ Hz and amplitude $H = 675$ A/m. Here, the spheres first are propelled downhill (negative X-direction, $\omega_H < 0$), and after a time t, the direction of field rotation was changed ($\omega_H > 0$) for the next time interval t. The values of t for these curves were $t = 60$ s, 30 s, 30 s, and 10 s (top to bottom). The less steep parts at the beginning or end of two of the curves marked as $H = 0$ correspond to no driving force, i.e., only gravity acting.

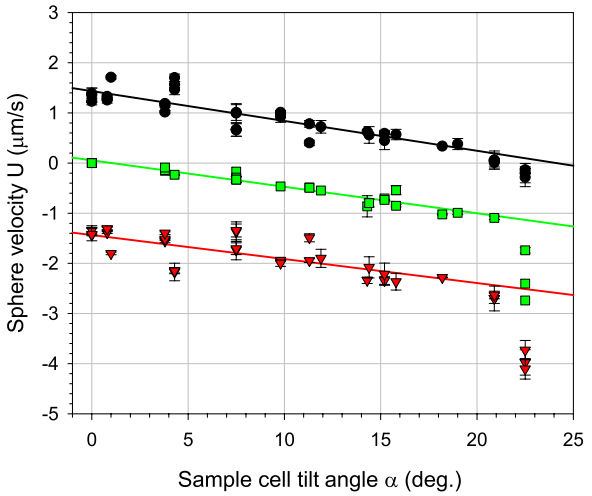

FIG. 6. The velocity of $d = 4.7\,\mu$m spheres being propelled uphill (black circles) or downhill (red triangles) by a $H = 675$ A/m field rotating at a frequency of 100 Hz for different values of the sample tilt angle α. The green squares show velocity of downhill sliding motion due to gravity. Solid lines are linear regression fits. Each data point represents several measurements using the same microsphere. For some tilt angles, two or three different particles were measured.

(red triangles), and also for spheres drifting freely downhill due to gravity only (green squares). As can be seen, there is some scattering of the data around three nearly parallel lines, with only minor deviations for the pure gravity case and largest deviations for the downhill motion data. The solid lines are linear regression fits to the three datasets in the angular range of $0° \le \alpha < 20°$, which may be considered the "small" tilt angle range. For tilt angle $\alpha = 22.5°$, the data fall clearly below these small tilt angle regression lines, and this is most clearly seen in the case of downhill rotation ($\Omega_y < 0$).

As expected from the linearization of Eq. (11) for small α, the data fall on three separate lines, which using linear regression can be approximated by

$$U_u(\alpha) = [1.43 - 0.059\alpha(\text{deg.})]\frac{\mu\text{m}}{\text{s}} = (1.43 - 3.4\alpha)\frac{\mu\text{m}}{\text{s}}, \tag{13}$$

$$U_d(\alpha) = [-1.43 - 0.048\alpha(\text{deg.})]\frac{\mu\text{m}}{s} = (-1.43 - 2.8\alpha)\frac{\mu\text{m}}{\text{s}}, \tag{14}$$

$$U_g(\alpha) = [-0.049\alpha(\text{deg.})]\frac{\mu\text{m}}{\text{s}} = -2.8\alpha\frac{\mu\text{m}}{\text{s}}, \tag{15}$$

for uphill (u), downhill (d), and pure gravitational (g) motion, respectively.

Now, first consider the case when only gravity is acting (middle curve of Fig. 6). Since the microspheres are in contact with the surface, it seems reasonable to assume that the microspheres are rolling downhill on the surface. Then, $\gamma = 1$ (pure rolling), $\mu_k = 0$, and $\varepsilon = -1$ (i.e., the component of gravity is in the direction of motion), and Eq. (11) gives $U_x = -U_s \cdot \frac{\sin\alpha}{f^t_{xx} - f^r_{xy}} \approx -U_s \cdot \frac{\alpha}{f^t_{xx} - f^r_{xy}}$ for small α. From the value of U_g in Eq. (15), one finds $\frac{U_s}{f^t_{xx} - f^r_{xy}} = 2.8\ \frac{\mu\text{m}}{\text{s}}$. Using the value of sedimentation velocity calculated above, $U_s = 9.0\,\mu$m/s, then $f^t_{xx} - f^r_{xy} = 3.2$, and from Eqs. (5) and (6), one finds that the effective separation between the surface of the spheres and the glass surface was $\delta \approx 16$ nm.

In order to check how this effective surface separation compares to the surface roughness of the microspheres, the surfaces of dry spheres deposited on a microscope slide were imaged using an atomic force microscope (AFM). A section of a typical AFM scanning image is shown in Fig. 1(d). As can be seen, the surface is not smooth on the nm-scale but looks bumpy with many protuberances. The scans showed local deviations from the spherical shape typically in the range of 5–30 nm. Based on such AFM scans, the surface roughness (locale deviation from spherical shape) can be estimated to about 20 nm (RMS-value). In a similar way, the surface of a microscope glass slide was checked and was much smoother with all protuberances well separated and typically less than 5 nm in height. These roughness results are in good agreement with the effective surface separation value found from the hydrodynamic interactions. Thus, the effective hydrodynamic separation of the surfaces in these experiments was $\delta \approx 15$–20 nm. Due to the larger protuberances, the spheres and the glass surface were in direct contact, and the frictional force was the main cause for propulsion when the magnetic torque was rotating the spheres.

For small tilt angles α, Eq. (11) can be linearized as $U_x(\alpha) = A + B \cdot \alpha$ with $A = \frac{\varepsilon\mu_k U_s}{f^t_{xx} - \frac{1}{\gamma} f^r_{xy}}$ and $B = -\frac{U_s}{f^t_{xx} - \frac{1}{\gamma} f^r_{xy}}$. Due to the scattering of the individual data points in Fig. 6, the slopes of the regression lines for uphill and downhill propulsion are equal within the statistical uncertainty, and their average value was used in the subsequent analysis. Based on the effective surface separation δ found above, the drag correction coefficients $f^t_{xx}(\delta)$ and $f^r_{xy}(\delta)$ were calculated. From this, the slipping coefficient γ for driven uphill or downhill motion was found to be $\gamma = 0.59$, and the angular rotation frequency of the microspheres was $\Omega_y(f_H = 100\,\text{Hz}) = U_x(\alpha = 0)/\,\gamma a = 1.1\ \text{s}^{-1}$. Using the expressions for A and B, the friction coefficient μ_k was found to be $\mu_k = |\frac{A}{B}| = 0.49$.

The regression lines in Fig. 6 are not good approximations to the experimental results for values of $\alpha > 20°$. However, due to the relative large scattering of data values, using the full expression Eq. (11) in the fitting and the whole range of α-values did not significantly change these results. As can be seen in Fig. 6, the uphill propulsion vanishes, $U_u = 0$, at about $\alpha \approx 21°$, and for larger tilt angles, even microspheres with positive Ω_y are slowly sliding downhill. Choosing $\alpha = \alpha_{\text{crit}} = 21°$ and using Eq. (12), the kinetic friction coefficient can be estimated to be $\mu_k \approx 0.51$, which is in quite good agreement with the value $\mu_k = 0.49$ found from the A/B-ratio. It may be noted that the exact values of slipping coefficient γ and angular velocity Ω_y depend on the effective separation δ between the microspheres and the glass surface. A 25% increase in the value of δ gives ~11% increase in γ and similar reduction in Ω_y.

For a fixed tilt angle, the main reasons for different average velocities of similar spheres are as follows: (i) the distribution of microsphere diameters d, which is about $\frac{\Delta d}{d} < 1.5\%$;[24] (ii) a variation in their induced magnetic moments m due to size variation and to the distribution of the magnetic material inside; and (iii) differences in the

effective sphere surface to glass surface separation caused by the surface roughness. Variation of velocity due to the glass surface could also easily be seen as "dirty" spots on the glass slowed down the speed or temporarily changed the direction of motion of the spheres. The velocity data were not used in such cases.

As seen in Fig. 6, in all three cases, the data measured for tilt angle $\alpha = 22.5°$ fall clearly below the linear approximation for the U_x-values, and the deviations are the largest for the pure gravity and $\Omega_y < 0$ data (green and red symbols). In fact, for this tilt angle, the velocity U_d of downhill propulsion exceeds the velocity due to pure rotational rolling $U_x = a\Omega_y \approx -2.6\ \mu$m/s for a sphere rotating at $\Omega_y \approx -1.1\ \text{s}^{-1}$, and the motion must be different from rolling/slipping and probably not described by Eq. (11).

The measured velocities for the horizontal sample ($\alpha = 0$) can be compared to those reported by Martinez-Pedrero *et al.*[8,9] who reported speeds of 0.6 μm/s and $\sim 1\ \mu$m/s for $d = 2.8\ \mu$m spheres at field rotation frequencies of 10 Hz and 150 Hz, respectively, using slightly higher field strength. These authors developed a model for the translational velocity of single particles and chains of particles purely based on the hydrodynamic interactions among the microspheres.[9] Based on their model and the experimental observations, they estimated a glass surface to sphere surface distance of $\delta \sim 180$ nm, which is considerably larger than the value found in the present study. In the model used in Ref. 9, the density difference between the microspheres and water was neglected, and it was assumed that double layer interactions keep surfaces separated. However, the density of the current microspheres was sufficiently large so that the spheres come in close contact to the glass surface. Since the lift forces are negligible for the low microsphere rotational velocities found here, a rolling/slipping model is the only pattern of motion that can explain the results found in the present experiments. The value of the friction coefficient $\mu_k \approx 0.5$ may seem higher than what one might expect since, e.g., the friction coefficient for dry polystyrene films sliding against steel has been reported to be $0.6 < \mu_k < 0.7$ (Ref. 30) and wetting a surface often reduces sliding friction considerably. Schiwek *et al.*[31] measured friction forces of nano-sized polystyrene spheres in water on a silicon wafer using AFM and reported that the adhesion was the strongest for pH = 6 and considerably lower for both higher and lower pH-values. Thus, properties of the substrate itself as well as the ionic strength of solution will influence adhesion and friction. It may be noted that the microscope slides were used without a specific cleaning procedure and a tendency of particles sticking to the surface increased with time.

The observed microsphere motion inside tilted samples opens up possibilities for using such setup for sorting of magnetic microspheres according to particle diameter or susceptibility, as particles with the largest magnetic moment will be able to travel the longest distance when the tilt angle of the sorting cell is slowly increased. Similar types of microbeads are commercially available as streptavidin coated particles that via the streptavidin-biotin reaction can be useful for cell separation and protein or nucleic acid purification.[32] Using mixtures of beads with different surface coatings, which can be attached to distinct cells or macromolecules, their mobility may depend on the attached cargo, and the differences in ability of the beads to move uphill can then be used for cell/molecule sorting.

V. CONCLUSION

Magnetic propulsion of paramagnetic microspheres near liquid-glass interfaces has been demonstrated. By applying magnetic fields rotating in a plane perpendicular to the interface, the magnetic particles in the liquid can be moved in a controlled way in a chosen direction. Using sample cells that are tilted relative to the horizontal direction, microspheres will move uphill, downhill, or be at fixed positions depending on the magnetic parameters (field strength and frequency), particle properties (diameter and susceptibility), the sample cell inclination, and the particle-surface contact friction coefficient. Propulsion speeds of 0.5–5 μm/s inside horizontal cells were found, and these speeds, as well as their tilt angle dependence, are in good agreement with what can be calculated from a rolling-slipping model of the sphere-surface contact with a friction coefficient $\mu_k \approx 0.50$, a slipping coefficient of about 0.6, and an effective distance between the spheres' surface and the glass surface of about 20 nm. The contact friction was partly due to protuberances on the microsphere surface. Such inclined cells containing surface-coated magnetic beads have potential use in biomedical separation, e.g., utilizing the streptavidin-biotin reaction to attach a molecular cargo.

SUPPLEMENTARY MATERIAL

See supplementary material for videos showing the motion of two microspheres inside a horizontal sample cell and one microsphere inside a tilted cell.

ACKNOWLEDGMENTS

The Computer Integrated Systems for Microscopy and Manipulation (CISMM) Center at University of North Carolina at Chapel Hill, supported by the NIH NIBIB, is gratefully acknowledged for making the Video Spot Tracker software freely available. A. T. Skjeltorp of IFE/Giamag (Norway) is acknowledged for many stimulating discussions and for useful comments to the manuscript.

[1]H. Bruus, *Theoretical Microfluidics* (Oxford University Press, Oxford, 2008).
[2]D. Xiao, T. Lu, R. Zeng, and Y. Bi, "Preparation and highlighted applications of magnetic microparticles and nanoparticles: A review on recent advances," Microchim. Acta **183**, 2655 (2016).
[3]J. Elgeti, R. G. Winkler, and G. Gompper, "Physics of microswimmers—single particle motion and collective behavior: A review," Rep. Prog. Phys. **78**, 056601 (2015).
[4]J. R. Blake and A. T. Chwang, "Fundamental singularities of viscous flow," J. Eng. Math. **8**, 23 (1974).
[5]S. Feng, A. L. Graham, J. R. Abbott, and H. Brenner, "Antisymmetric stresses in suspensions: Vortex viscosity and energy dissipation," J. Fluid. Mech. **563**, 97 (2006).
[6]R. D. Leonardo, D. D. Arciprete, L. Angelani, and V. Iebba, "Swimming with an image," Phys. Rev. Lett. **106**, 038101 (2011).
[7]X. J. A. Janssen, A. J. Schellekens, K. van Ommering, L. J. van Ijzendoorn, and M. W. J. Prins, "Controlled torque on superparamagnetic beads for functional biosensors," Biosens. Bioelectron. **24**, 1937 (2009).

[8]F. Martinez-Pedrero and P. Tierno, "Magnetic propulsion of self-assembled colloidal carpets: Efficient cargo transport via a conveyor-belt effect," Phys. Rev. Appl. **3**, 051003 (2015).
[9]F. Martinez-Pedrero, A. Ortiz-Ambriz, I. Pagonabarraga, and P. Tierno, "Colloidal microworms propelling via a cooperative hydrodynamic conveyor belt," Phys. Rev. Lett. **115**, 138301 (2015).
[10]T. O. Tasci, P. S. Herson, K. B. Neeves, and D. W. M. Marr, "Surface-enabled propulsion and control of colloidal microwheels," Nat. Commun. **7**, 10225 (2016).
[11]Y. Fily, A. Baskaran, and M. C. Marchetti, "Cooperative self-propulsion of active and passive rotors," Soft Matter **8**, 3002 (2012).
[12]C. E. Sing, L. Schmid, M. F. Schneider, T. Franke, and A. Alexander-Katz, "Controlled surface-induced flows from the motion of self-assembled colloidal walkers," Proc. Natl. Acad. Sci. U.S.A. **107**, 535 (2010).
[13]H. Morimoto, T. Ukai, Y. Nagaoka, N. Grobert, and T. Maekawa, "Tumbling motion of magnetic particles on a magnetic substrate induced by a rotational magnetic field," Phys. Rev. E **78**, 021403 (2008).
[14]A. R. Kose, B. Fischer, L. Mao, and H. Koser, "Label-free cellular manipulation and sorting via biocompatible ferrofluids," Proc. Natl. Acad. Sci. U.S.A. **106**, 21478 (2009).
[15]R. M. Erb, J. J. Martin, R. Soheilian, C. Pan, and J. R. Barber, "Actuating soft matter with magnetic torque," Adv. Funct. Mater. **26**, 3859 (2016).
[16]J. R. Smart, S. Beimfohr, and D. T. Leighton, Jr., "Measurement of the translational and rotational velocities of a noncolloidal sphere rolling down a smooth inclined plane at low Reynolds number," Phys. Fluids A **5**, 13 (1993).
[17]K. P. Galvin, Y. Zhao, and R. H. Davis, "Time-averaged hydrodynamic roughness of a noncolloidal sphere in low Reynolds number motion down an inclined plane," Phys. Fluids **13**, 3108 (2001).
[18]P. Cherukat and J. B. Mclaughlin, "The inertial lift on a rigid sphere in a linear shear flow field near a flat wall," J. Fluid Mech. **263**, 1 (1994).
[19]G. P. Krishnan and D. T. Leighton, "Inertial lift on a moving sphere in contact with a plane wall in a shear flow," Phys. Fluids **7**, 2538 (1995).
[20]M. R. King and D. T. Leighton, "Measurement of the inertial lift on a moving sphere in contact with a plane wall in a shear flow," Phys. Fluids **9**, 1248 (1997).
[21]R. D. Duffadar and J. M. Davis, "Interaction of micrometer-scale particles with nanotextured surfaces in shear flow," J. Colloid Interface Sci. **308**, 20 (2007).
[22]R. R. Agayan, R. G. Smith, and R. Kopelman, "Slipping friction of an optically and magnetically manipulated microsphere rolling at a glass-water interface," J. Appl. Phys. **104**, 054915 (2008).
[23]M. M. Rashidi, S. Johnson, and Z. Yang, "Theoretical study of moving magnetic beads on an inclined plane and its application in the ratchet separation technique," J. Magn. Magn. Mater. **398**, 13 (2016).
[24]G. Fonnum, C. Johansson, A. Molteberg, S. Mørup, and E. Aksnes, "Characterization of Dynabeads by magnetization measurements and Mössbauer spectroscopy," J. Magn. Magn. Mater. **293**, 41 (2005).
[25]G. Helgesen, P. Pieranski, and A. T. Skjeltorp, "Nonlinear phenomena in systems of magnetic holes," Phys. Rev. Lett. **64**, 1425 (1990).
[26]G. Helgesen and A. T. Skjeltorp, "An experimental system for studying dynamic behavior of magnetic microparticles," J. Appl. Phys. **69**, 8277 (1991).
[27]M. Chaoui and F. Feuillebois, "Creeping flow around a sphere in a shear flow close to a wall," Q. J. Mech. Appl. Math. **56**, 381 (2003).
[28]A. J. Goldman, R. G. Cox, and H. Brenner, "Slow viscous motion of a sphere parallel to a plane wall. Part I. Motion through a quiescent fluid," Chem. Eng. Sci. **22**, 637 (1967).
[29]Q. Liu and A. Prosperetti, "Wall effects on a rotating sphere," J. Fluid Mech. **657**, 1 (2010).
[30]W. Liu, S. Yang, C. Li, and Y. Sun, "Friction and wear behaviour of carbon ion-implanted PS against steel," Thin Solid Films **323**, 158 (1998).
[31]S. Schiwek, L.-O. Heim, R. W. Stark, and C. Dietz, "Manipulation of polystyrene nanoparticles on a silicon wafer in the peak force tapping mode in water: pH-dependent friction and adhesion force," J. Appl. Phys. **117**, 104303 (2015).
[32]D. Dressman, H. Yan, G. Traverso, K. W. Kinzler, and B. Vogelstein, "Transforming single DNA molecules into fluorescent magnetic particles for detection and enumeration of genetic variations," Proc. Natl. Acad. Sci. U.S.A. **100**, 8817 (2003).